

# Coupling Interface Constructions of MoS<sub>2</sub>/Fe<sub>5</sub>Ni<sub>4</sub>S<sub>8</sub> Heterostructures for Efficient Electrochemical Water Splitting

Yi Wu, Fan Li, Wenlong Chen, Qian Xiang, Yanling Ma, Hong Zhu,\* Peng Tao, Chengyi Song, Wen Shang, Tao Deng, and Jianbo Wu\*

Water splitting is considered as a pollution-free and efficient solution to produce hydrogen energy. Low-cost and efficient electrocatalysts for the hydrogen evolution reaction (HER) and the oxygen evolution reaction (OER) are needed. Recently, chemical vapor deposition is used as an effective approach to gain high-quality MoS<sub>2</sub> nanosheets (NSs), which possess excellent performance for water splitting comparable to platinum. Herein, MoS<sub>2</sub> NSs grown vertically on FeNi substrates are obtained with in situ growth of Fe<sub>5</sub>Ni<sub>4</sub>S<sub>8</sub> (FNS) at the interface during the synthesis of MoS<sub>2</sub>. The synthesized MoS<sub>2</sub>/FNS/FeNi foam exhibits only 120 mV at 10 mA cm<sup>-2</sup> for HER and exceptionally low overpotential of 204 mV to attain the same current density for OER. Density functional theory calculations further reveal that the constructed coupling interface between MoS<sub>2</sub> and FNS facilitates the absorption of H atoms and OH groups, consequently enhancing the performances of HER and OER. Such impressive performances herald that the unique structure provides an approach for designing advanced electrocatalysts.

With the increasing concern on the exhausting of fossil fuel and pollution of environment, it is critical to search for cheap, clean, and efficient energy resources in order to meet the demand of exploration of new materials, advancing technologies, and growing population. Hydrogen, which is expected to substitute the current energy source, is a contamination-free

Y. Wu, F. Li, W. Chen, Q. Xiang, Y. Ma, Prof. H. Zhu, Prof. P. Tao, Prof. C. Song, Prof. W. Shang, Prof. T. Deng, Prof. J. Wu  
State Key Laboratory of Metal Matrix Composites

School of Materials Science and Engineering

Hydrogen Science Research Center

Shanghai Jiao Tong University

800 Dongchuan Road, Shanghai 200240, P. R. China

E-mail: hong.zhu@sjtu.edu.cn; jianbowu@sjtu.edu.cn

Prof. H. Zhu

University of Michigan - Shanghai Jiao Tong University Joint Institute

Shanghai Jiao Tong University


800 Dongchuan Road, Shanghai 200240, P. R. China

Prof. H. Zhu, Prof. J. Wu

Materials Genome Initiative Center

Shanghai Jiao Tong University

800 Dongchuan Road, Shanghai 200240, P. R. China

 The ORCID identification number(s) for the author(s) of this article can be found under <https://doi.org/10.1002/adma.201803151>.

DOI: 10.1002/adma.201803151

fuel and the most promising energy carrier with high gravimetric energy density.<sup>[1]</sup> Water splitting is considered as one of the most promising routes for hydrogen production.<sup>[2–4]</sup> The electrochemical oxygen evolution reaction (OER) and hydrogen evolution reaction (HER) are the two critical processes for water splitting. However, these two key reactions are still hindered by many factors, in which the activity of catalyst cannot be ignored.<sup>[5]</sup> Therefore, tremendous efforts have been made to find a proper catalyst to gain an efficient water splitting. Platinum (Pt) is one of the excellent catalysts, but the expensive price and scarce content on earth limit its extensive application in water splitting.<sup>[6]</sup> Henceforth, it is in urgent need to explore efficient alternatives.

The 2D materials hold massive advantages including high-specific area and special in-plane electron transfer mode.<sup>[7,8]</sup> Molybdenum disulfide (MoS<sub>2</sub>) is considered to be a promising material for HER, which has been proved by both experimental results and theoretical calculations.<sup>[9–13]</sup> Particularly, the hydrogen adsorption energy of the sulfur atoms at the edge of 2D MoS<sub>2</sub> NSs approaches zero, indicating its latent application comparable to Pt.<sup>[14]</sup> Generally, the active sites of MoS<sub>2</sub> NSs also contain sulfur vacancies in the basal plane according to recent studies.<sup>[15,16]</sup> Furthermore, 2D MoS<sub>2</sub> NSs have been synthesized by several common methods, such as physical exfoliation,<sup>[7,17]</sup> chemical exfoliation,<sup>[7,17,18]</sup> hydrothermal process,<sup>[7,19,20]</sup> and atomic layer deposition.<sup>[21]</sup> Chemical vapor deposition (CVD) is also recognized as an available method to gain high-quality MoS<sub>2</sub> NSs which others do not possess.<sup>[7,9,13,22–26]</sup>

Meanwhile, at the OER side, iron- and nickel-based compounds show an outstanding performance in OER according to the recent researches.<sup>[27–31]</sup> With abundant active sites, large-specific area and high electrical conductivity, iron-nickel alloy (FeNi) foam can be a promising candidate for efficient OER.

For boosting both reactions toward water splitting, recent researches focus on various methods, including integrating the superiorities of HER-efficient materials and OER-efficient materials,<sup>[2,32]</sup> increasing the conductivity,<sup>[3]</sup> and raising the surface area,<sup>[4]</sup> etc. Therefore, building novel heterostructures possessing coupling interfaces of efficient HER and OER catalysts is a promising direction.

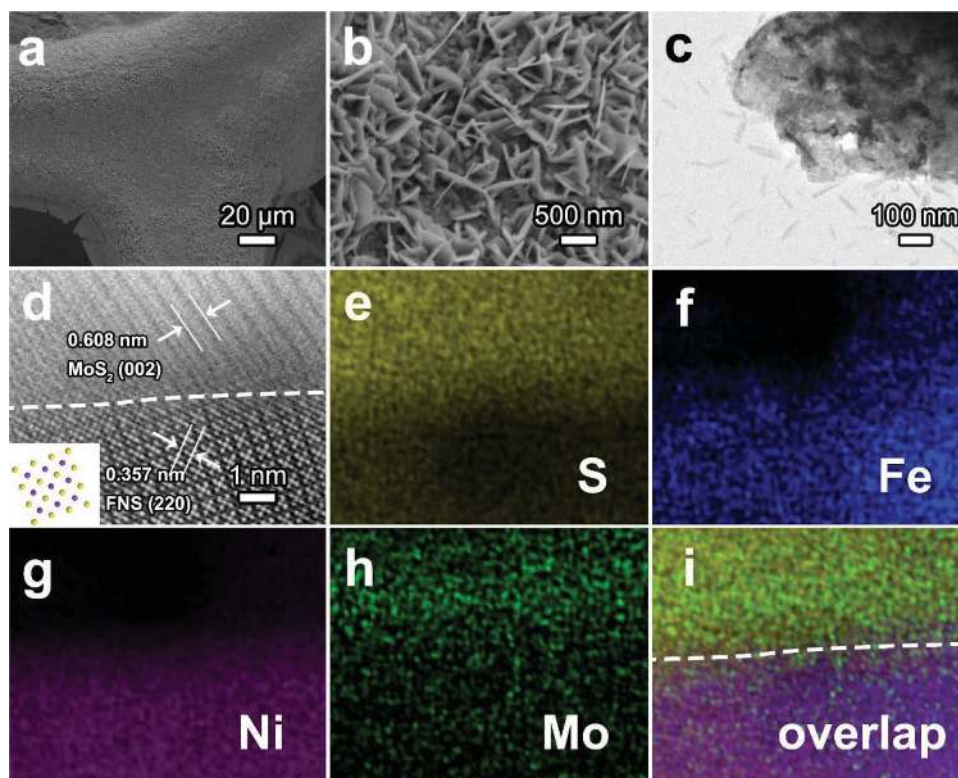


**Figure 1.** Morphology characterizations of MoS<sub>2</sub>/FNS/FeNi foam. a,b) SEM of vertically grown MoS<sub>2</sub>/FNS heterostructures with different magnification. c) Low-magnification TEM microscopic image of MoS<sub>2</sub>/FNS heterostructures. d) Atomic-resolution HAADF-STEM image of MoS<sub>2</sub>/FNS interface. The inset in panel (d) indicates the atomic model of FNS, the yellow balls represent S atoms and the purple balls stand for Fe/Ni atoms. e–i) The high-resolution EDX elements maps of panel (d). The dash white lines highlight the interfaces between MoS<sub>2</sub> and FNS.

In this study, we demonstrate the heterostructures of MoS<sub>2</sub> and FeNi substrate as a promising electrode for bicalysis of HER and OER. We found the in situ grown FNS layer induces the strong couple interaction at the interface, which is responsible for an extremely low overpotential of 120 mV for HER and 204 mV for OER at 10 mA cm<sup>-2</sup>.

The CVD synthesis of MoS<sub>2</sub> on different substrates (300 nm SiO<sub>2</sub>/Si, fluorin-doped tin oxide (FTO), FeNi foam, and FeNi foil) is illustrated as Figure S1 in the Supporting Information. Herein, we use a three-temperature-zone furnace to control the exact temperature of each precursor. Before CVD, 500 sccm N<sub>2</sub> is pumped through the tube for 30 min to make sure the emission of air which is essential for the next step.<sup>[24]</sup>

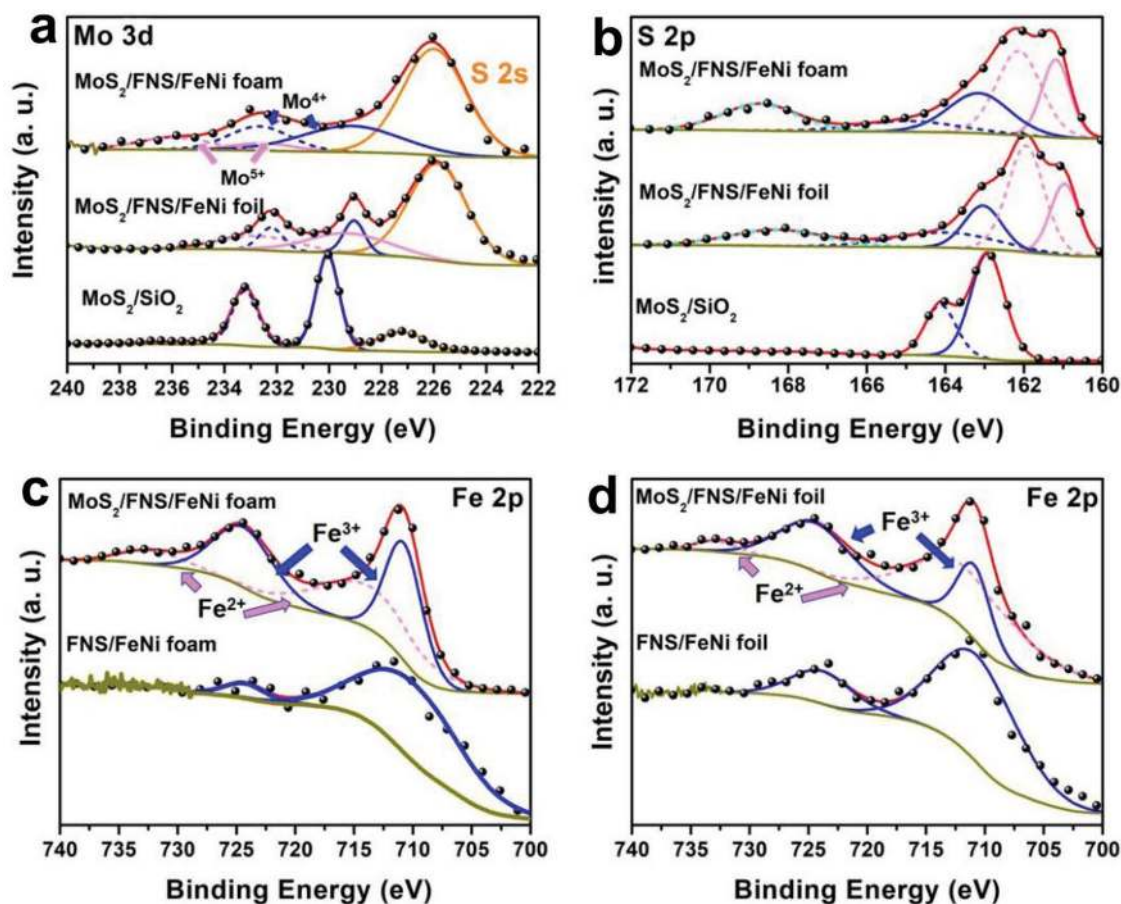
Figure S2 in the Supporting Information presented the scanning electron microscopy (SEM) images of pure FeNi foam and FeNi foam/Fe<sub>5</sub>Ni<sub>4</sub>S<sub>8</sub> (FNS) with the unsmooth surface. **Figure 1a,b** demonstrated the vertical growth mode and the uniform dispersity of MoS<sub>2</sub> array deposited on FeNi foam. The size and thickness of the MoS<sub>2</sub> NSs were 300–400 and 10–20 nm. X-ray diffraction shows the peaks at 43.6°, 50.79°, and 74.67° for Fe<sub>0.64</sub>Ni<sub>0.36</sub> alloy, 29.32°, 35.55°, and 57.72° for FNS, respectively (Figure S3a, Supporting Information). Due to the high signal of FeNi, the X-ray diffraction of MoS<sub>2</sub>/FNS powder, which was peeled off from the FeNi substrate by sonication, was carried out to reveal the existence of MoS<sub>2</sub> with the characteristic peak at 14.4° (Figure S3b, Supporting Information), corresponding to the (002) plane with the spacing of 0.615 nm. The high-resolution transmission electronic microscopy (TEM)

images of MoS<sub>2</sub>/FNS show the lattice of 0.615 nm, which is consistent with the MoS<sub>2</sub> (002) plane (Figure S4a–c, Supporting Information). At the interface, the lattice spacings of 0.206 and 0.505 nm correspond to the (422) and (200) facets of FNS, respectively, while the spacings of 0.228, 0.615, and 0.273 nm were ascribed to the (103), (002), and (100) planar of MoS<sub>2</sub>, respectively (Figure S4d–f, Supporting Information). The MoS<sub>2</sub> (105) and the FNS (220) can also be observed by atomic-resolution high angle annular dark field scanning TEM (HAADF-STEM) imaging (Figure S4g–i, Supporting Information). The interfaces of MoS<sub>2</sub>/FNS were also revealed by the HAADF-STEM (Figure 1d). The corresponding energy dispersive X-ray (EDX) element mapping (Figure 1e–i) shows that Fe and Ni elements are homogeneously distributed on the bottom while the Mo element is scattered on the top, which confirms the interface construction. The fast Fourier transform (FFT) patterns further indicate the interface of MoS<sub>2</sub> and FNS (Figure S5, Supporting Information). The interfaces were also observed from the EDX mapping of the top view of MoS<sub>2</sub> on FNS (Figure S6, Supporting Information). We observed this MoS<sub>2</sub>/FNS interface in various structural characterizations (Figure 1d,i, Figure S4d–f,S5, and Figure S6, Supporting Information), suggesting the widely existence of this interface coupling. It is worth noting that vertical growth behavior of MoS<sub>2</sub> on FeNi foam is quite different from that on SiO<sub>2</sub>/Si plates, on which MoS<sub>2</sub> sheets only grew horizontally (Figure S7, Supporting Information). These differences of growth behavior stem from the rough surface of FeNi foam with numerous

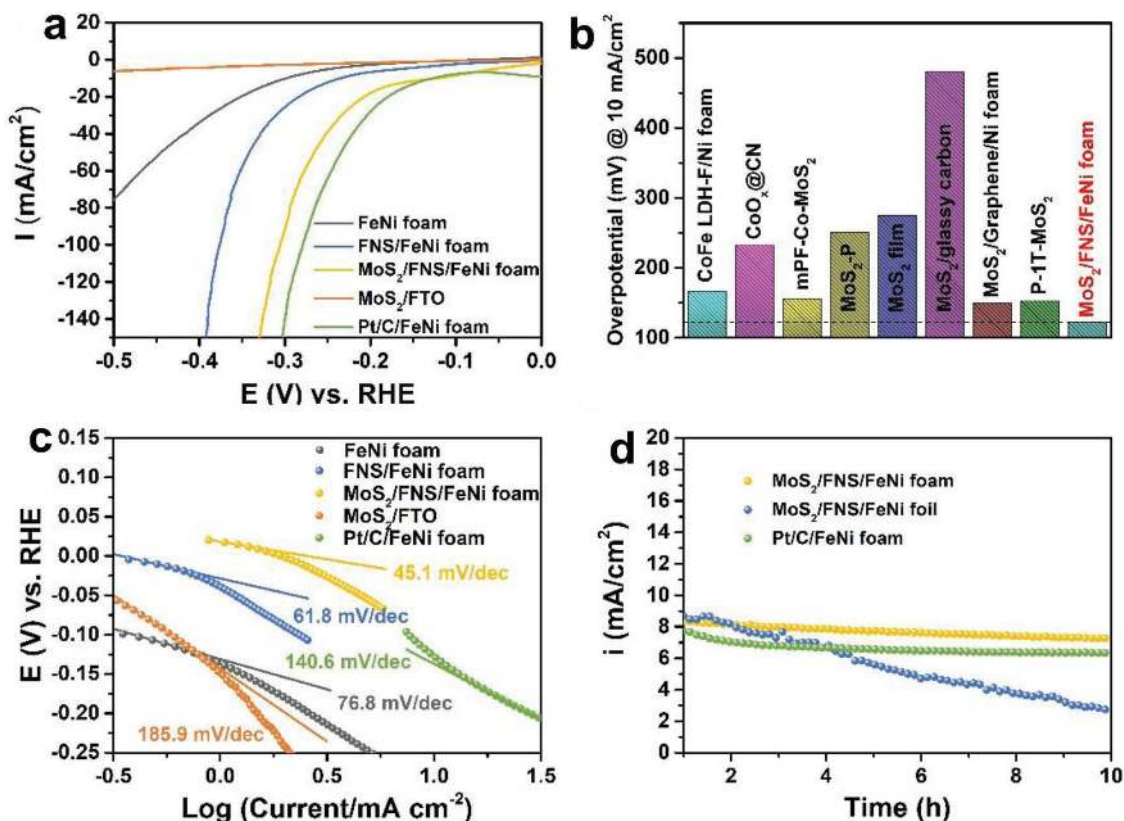
nucleation sites.<sup>[9,28]</sup> The MoS<sub>2</sub> NSs can further be modified through control of the deposition time (Figure S8, Supporting Information). We found that the MoS<sub>2</sub> NSs became larger but thinner as the reaction time increased from 10 to 60 min (Figure S8, Supporting Information). The size increased from ≈350 nm to ≈1 μm and the thickness decreased from ≈15 nm to ≈3 nm. SEM-EDX analysis shows MoS<sub>2</sub> deposited FeNi foam consists of Mo, S, Fe, and Ni (Figure S9, Supporting Information). Furthermore, elemental mapping was performed to verify that the Fe, Ni, Mo, and S elements are found to be evenly distributed on the FeNi foam (Figure S10, Supporting Information). Using the similar process, we also grew MoS<sub>2</sub> 2D sheets array on FeNi foil, which is directly confirmed by SEM (Figure S11, Supporting Information). The Raman spectroscopy shows two characteristic peaks at 383 cm<sup>-1</sup> and 405 cm<sup>-1</sup> (Figure S12, Supporting Information). The two characteristic peaks correspond to the in-plane vibration and out-of-plane vibration modes for MoS<sub>2</sub>, respectively. The gap between the peaks shows that the MoS<sub>2</sub> NSs are not monoatomic layer, which is consistent with the SEM results.<sup>[13,23,24]</sup>

Figure 2 and Figure S13 in the Supporting Information presented X-ray photoelectron spectroscopy (XPS) patterns of MoS<sub>2</sub>/FNS/FeNi substrates. The bottom curve of Figure 2a showed two peaks of Mo 3d spectra located at 230.1 and 233.2 eV, which can be assigned to the Mo 3d 5/2 and

Mo 3d 3/2, confirming the existence of Mo<sup>4+</sup> in MoS<sub>2</sub>/SiO<sub>2</sub>.<sup>[13]</sup> For MoS<sub>2</sub>/FNS/FeNi foam or foil, these two feature peaks shift negatively to 229.1 and 232.3 eV, respectively, implying the strong electronic interactions between FNS and MoS<sub>2</sub>.<sup>[2]</sup> This interaction has been demonstrated in the system of MoS<sub>2</sub>/Ni<sub>3</sub>S<sub>2</sub>.<sup>[2]</sup> The pink peaks show the appearance of Mo<sup>6+</sup> and the orange peak at 226 eV belongs to S 2s.<sup>[28,33]</sup> In the S 2p spectrum of Figure 2b, the fitted peaks of MoS<sub>2</sub>/SiO<sub>2</sub> located at 162.9 and 164.0 eV can be assigned to the S 2p 3/2 and S 2p 1/2, which indicates the oxidation state of S<sup>2-</sup>.<sup>[28]</sup> The presence of S 2p peaks at 168.5 eV of MoS<sub>2</sub> on FeNi substrates demonstrates the substrates sulfurization and the presence of S 2p peaks at 161.9 and 160.9 eV shows the existences of bridging S<sub>2</sub><sup>2-</sup> or apical S<sup>2-</sup>.<sup>[2,33]</sup> For the SiO<sub>2</sub> substrate, the atomic ratio of Mo and S of MoS<sub>2</sub>/SiO<sub>2</sub> is ≈2:1 by comparing the total areas of the corresponding orbit proportioned to atomic sensitivity factor.<sup>[33]</sup> For FeNi substrates, the atomic ratios of Mo and S are 0.13 and 0.18 for foil and foam, respectively. The excess S can be attributed to the formation of FNS. Figure 2c,d shows the appearance of Fe<sup>2+</sup> after MoS<sub>2</sub> deposition on FeNi substrates.<sup>[34]</sup> Meanwhile, the binding energy of Ni 2p peaks shifts positively after the deposition of MoS<sub>2</sub> on FeNi substrates meaning the electronic reciprocity between FNS and MoS<sub>2</sub>, corresponding to the result of Mo 3d (Figure 2a), which strongly demonstrates the existence of coupling interfaces between MoS<sub>2</sub> and FNS.<sup>[2,35]</sup>



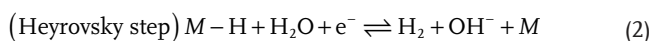
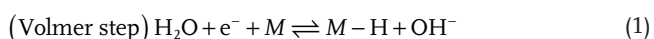
**Figure 2.** XPS of MoS<sub>2</sub>/FNS. a) Mo 3d, b) S 2p, c) Fe 2p of MoS<sub>2</sub>/FNS/FeNi foam, and d) Fe 2p of MoS<sub>2</sub>/FNS/FeNi foil. The black dots are original data, the brown curves are background and the blue, red, orange, and pink lines are the fitted curves.



**Figure 3.** HER performances of MoS<sub>2</sub>/FNS/FeNi foam, FNS/FeNi foam, FeNi foam, and MoS<sub>2</sub>/FTO with the three-electrode system in 1 M KOH aqueous electrolyte. a) Polarization curves, b) HER overpotentials of the MoS<sub>2</sub>/FNS/FeNi foam and the reported catalysts for comparison at 10 mA cm<sup>-2</sup>, c) corresponding Tafel slopes for HER, and d) chronoamperometric curves of MoS<sub>2</sub>/FNS/FeNi foam at -122 mV and MoS<sub>2</sub>/FNS/FeNi foil at -281 mV.

The HER activities of MoS<sub>2</sub> grown on FeNi substrates and FTO were evaluated in 1.0 M KOH. **Figure 3a** shows the HER performances of MoS<sub>2</sub> NSs on different substrates. The MoS<sub>2</sub> sheets array on FeNi foam showed a supreme HER performance compared to FeNi foam, FNS/FeNi foam, and MoS<sub>2</sub>/FTO. Moreover, we dissolved the samples containing MoS<sub>2</sub> for inductively coupled plasma (ICP) tests. For MoS<sub>2</sub>/FNS/FeNi foam, even at a low mass loading (0.153 mg cm<sup>-2</sup>), the specific activity of MoS<sub>2</sub> can reach 252.7 mA mg<sup>-1</sup> at the overpotential of 250 mV (Table S1, Supporting Information). Among non-noble metal catalysts, the MoS<sub>2</sub>/FNS/FeNi foam showed low onset overpotentials of 30 mV (Figure 3a). Moreover, the 122 mV overpotential at 10 mA cm<sup>-2</sup> of MoS<sub>2</sub>/FNS/FeNi foam is extraordinarily small compared with FNS/FeNi foam (≈236 mV), pure FeNi foam (≈299 mV), MoS<sub>2</sub>/FTO (≈615 mV), recently reported data (Figure 3b and Table S2, Supporting Information),<sup>[3,4,9,11,13,16,28,33]</sup> and even Pt/C/FeNi foam (≈127 mV). These results can demonstrate that the exposed edge sites of MoS<sub>2</sub> and the coupling interfaces between MoS<sub>2</sub> and FNS are critical factors to this small overpotential for HER.

For HER in alkaline solution, water reduction is described by the following three steps<sup>[36]</sup>:



where *M* denotes the surface empty site.

Tafel slopes of 120, 40, and 30 mV dec<sup>-1</sup> were observed for Volmer, Heyrovsky, and Tafel determining steps, respectively.<sup>[36]</sup>

The Tafel curves (Figure 3c) gained from the LSV curves of HER (Figure 3a) showed a slope of 45.1 mV dec<sup>-1</sup> for MoS<sub>2</sub>/FNS/FeNi foam, which is much smaller than 61.8 mV dec<sup>-1</sup> for FNS/FeNi foam, 76.8 mV dec<sup>-1</sup> for FeNi foam, and 185.9 mV dec<sup>-1</sup> for MoS<sub>2</sub>/FTO. Such a Tafel slope of MoS<sub>2</sub>/FNS/FeNi foam suggests a combined Volmer–Heyrovsky mechanism for hydrogen evolution.<sup>[36]</sup>

Furthermore, we also tested HER of MoS<sub>2</sub>/FNS/FeNi foil (Figure S14, Supporting Information). The overpotentials of the MoS<sub>2</sub>/FNS/FeNi foil are substantially lower than that of FNS/FeNi foil, FeNi foil and MoS<sub>2</sub>/FTO at 10, 20, and 50 mA cm<sup>-2</sup>, exhibiting the same trend as the samples on foam (Table S1, Supporting Information). These results demonstrate that MoS<sub>2</sub>/FNS coupling interfaces indeed enhance the HER reaction kinetics. In addition, the electrochemical impedance spectroscopy (EIS) was conducted at the overpotential of 250 mV to review the electrode kinetics of MoS<sub>2</sub>/FNS/FeNi substrates in the HER process (Figure S15, Supporting Information). Smaller charge transfer resistances (*R<sub>ct</sub>*) were obtained after MoS<sub>2</sub> deposition (from 6.0 Ω to 4.0 Ω for FeNi foam; from 41.2 Ω to 24.3 Ω for FeNi foil), which indicates the faster electron transfer process was obtained after the MoS<sub>2</sub> deposition during HER.

Furthermore, MoS<sub>2</sub>/FNS/FeNi foam holds the reduction of overpotential at the same current density relative to that of MoS<sub>2</sub>/FNS/FeNi foil and MoS<sub>2</sub>/FTO. The modest object conductivity of MoS<sub>2</sub>/FTO is an apparent bottleneck that inhibits the MoS<sub>2</sub> achieving the inherently high mass activity observed on FeNi substrates (Table S1, Supporting Information). These results demonstrate that the improved performance at lower MoS<sub>2</sub> loading can be attributed to the cooperation of high-specific activity of MoS<sub>2</sub> and highly-conductive substrates.

Amperometric *i*-*t* curves were performed to further evaluate the HER stability of MoS<sub>2</sub>/FNS/FeNi substrates (Figure 3d). The HER activity retained steady (72.6%) with 10 hours from 10 mA cm<sup>-2</sup> for MoS<sub>2</sub>/FNS/FeNi foam, which is remarkably better than the 63.2% after 10 h for Pt/C/FeNi foam, indicating the strong coupling interfaces and HER stability of MoS<sub>2</sub>/FNS heterostructures.

OER performances of MoS<sub>2</sub>/FNS/FeNi foam, FNS/FeNi foam, pure FeNi foam, MoS<sub>2</sub>/FTO, and IrO<sub>2</sub>/FeNi foam were studied in 1 M O<sub>2</sub>-saturated KOH electrolyte through cyclic voltammetry (CV) at a scan rate of 1 mV s<sup>-1</sup> (Figure 4a). The backward curves of CV test showed that the MoS<sub>2</sub>/FNS/FeNi foam exhibits much lower overpotentials at 10, 20, and 50 mA cm<sup>-2</sup> than those of other samples. Typically, as to OER, we took FNS and IrO<sub>2</sub> for active materials relative to MoS<sub>2</sub>.<sup>[37]</sup> The actual mass of FNS has been confirmed by ICP results for

MoS<sub>2</sub>/FNS/FeNi, and the specific mass activity of MoS<sub>2</sub>/FNS/FeNi foam is 63 times larger than that of FNS/FeNi foam and 82 times larger than that of IrO<sub>2</sub>/FeNi foam at the overpotential of 250 mV (Table S3, Supporting Information). Significantly, reaching 10 mA cm<sup>-2</sup> requires extremely low overpotential of 204 mV (Figure 4b), which outperformed FNS/FeNi foam (ca. 265 mV), FeNi foam (≈288 mV), MoS<sub>2</sub>/FTO (≈674 mV), commercial IrO<sub>2</sub>/FeNi foam (≈308 mV), and the previous reported works (see the details in Table S4 in the Supporting Information).<sup>[2-4,21,27,30,38-42]</sup> (Figure 4b). We can deduce that the MoS<sub>2</sub> deposition indeed improves the OER kinetics.

Figure 4c illustrates that the Tafel slopes of MoS<sub>2</sub>/FNS/FeNi foam is 28.6 mV dec<sup>-1</sup>, which is lower than that of the FNS/FeNi foam (≈43.3 mV dec<sup>-1</sup>), the FeNi foam (≈42.8 mV dec<sup>-1</sup>), and the MoS<sub>2</sub>/FTO (≈100.9 mV dec<sup>-1</sup>), implying a rapid OER reaction rate of MoS<sub>2</sub>/FNS/FeNi foam. These results demonstrate the coupling interfaces activate the water-oxidation reaction kinetics.<sup>[2,36]</sup>

The OER performance of MoS<sub>2</sub>/FNS/FeNi foil was also tested to give further investigation (Figure S16, Supporting Information). From the backward curves of MoS<sub>2</sub>/FNS/FeNi foil, FNS/FeNi foil, FeNi foil, and MoS<sub>2</sub>/FTO, the MoS<sub>2</sub>/FNS/FeNi foil shows the lower overpotentials than that of the others at 10, 20, and 50 mA cm<sup>-2</sup>, which shows the same trend as FeNi foam substrate. Meanwhile, MoS<sub>2</sub>/FNS/FeNi foam exhibits the

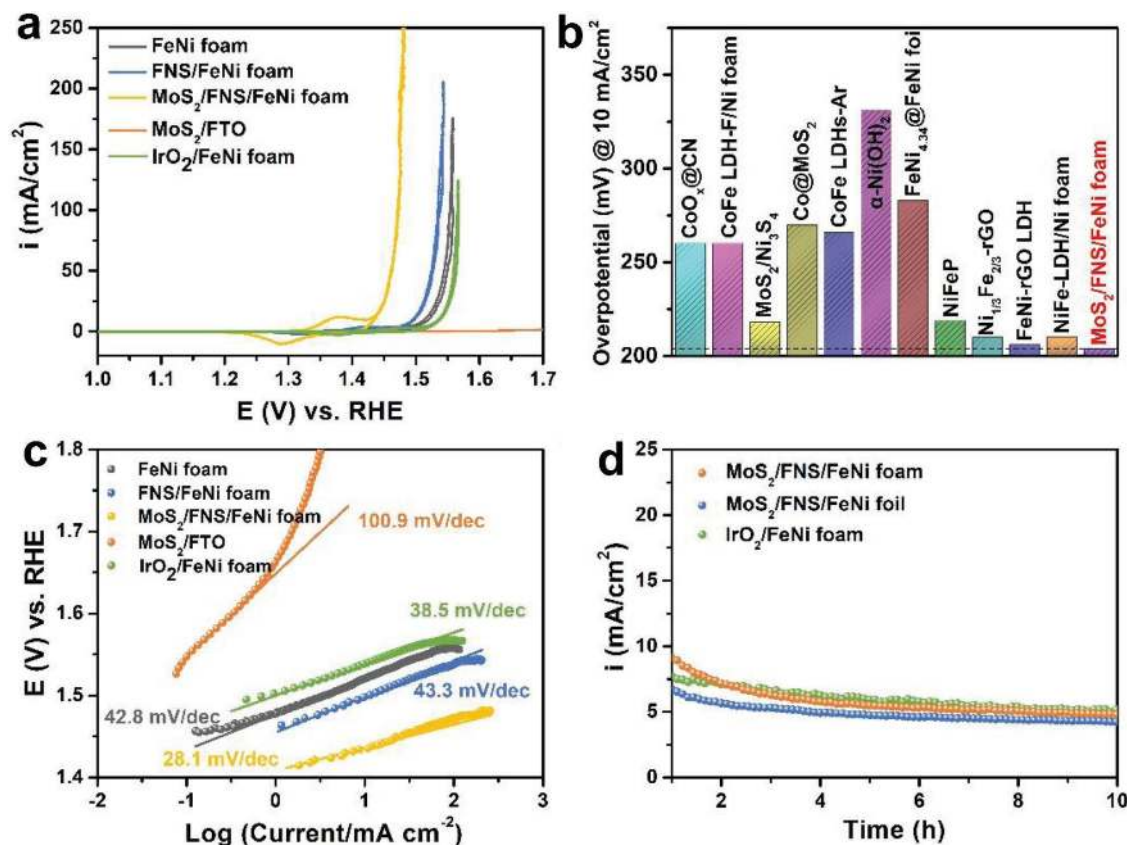


**Figure 4.** OER performances of MoS<sub>2</sub>/FNS/FeNi foam, FNS/FeNi foam and MoS<sub>2</sub>/FTO with the three-electrode system in 1 M KOH aqueous electrolyte. a) CV curves, b) OER overpotentials of the MoS<sub>2</sub>/FNS/FeNi foam and the reported catalysts for comparison at 10 mA cm<sup>-2</sup>, c) corresponding Tafel slopes for OER from backward curves of CV, and d) chronoamperometric curves of MoS<sub>2</sub>/FNS/FeNi foam at 204 mV and MoS<sub>2</sub>/FNS/FeNi foil at 251 mV.

lower overpotential at the same current density relative to that of MoS<sub>2</sub>/FNS/FeNi foil and MoS<sub>2</sub>/FTO. The specific activity of MoS<sub>2</sub>/FNS/FeNi foam shows 565.2 mA mg<sup>-1</sup> at the overpotential of 250 mV (Table S3, Supporting Information). Therefore, we conclude that the growth of MoS<sub>2</sub> on FeNi foam is critical for the improvement of OER performances. Moreover, EIS measurement was carried out at 1.48 V to reveal that the charge transfer resistance (*R*<sub>ct</sub>) values of MoS<sub>2</sub>/FNS/FeNi substrates (1.7 Ω for foam and 3.5 Ω for foil) are lower than pure FeNi substrates (3.6 Ω for foam and 7.0 Ω for foil), which indicates that the faster electron transfer during OER after MoS<sub>2</sub> deposition (Figure S17, Supporting Information).

The stability of MoS<sub>2</sub>/FNS/FeNi foam and foil were conducted at 204 mV and 251 mV for 10 h, respectively, and no apparent decay happened, which is comparable to the IrO<sub>2</sub>/FeNi foam (Figure 4d), indicating the vertically grown MoS<sub>2</sub> array on FeNi foam with coupling interfaces is stable even after 10 h of oxygen release.

We further elucidate the origin of constructed coupling interfaces of MoS<sub>2</sub>/FNS on enhancing the HER and OER by DFT calculations (see the details in DFT methods of Supporting Information). The adsorption energy for H on MoS<sub>2</sub> (103), Fe/Ni atoms doped MoS<sub>2</sub> (FeNi-MoS<sub>2</sub>) (103), OH on Fe<sub>9</sub>S<sub>8</sub> (422), Ni<sub>9</sub>S<sub>8</sub> (422), Mo atoms doped Fe<sub>9</sub>S<sub>8</sub> (Mo-Fe<sub>9</sub>S<sub>8</sub>) (422), and Mo atoms doped Ni<sub>9</sub>S<sub>8</sub> (Mo-Ni<sub>9</sub>S<sub>8</sub>) (422) were calculated (Figure 5a). Compared to the chemisorption energy on the (103) of MoS<sub>2</sub> surfaces ( $\Delta G_{\text{H}} = -0.649$  eV), the H atoms chemisorption energy of (103) surfaces at S edge sites of FeNi-MoS<sub>2</sub> is just -1.575 eV, which results in the inclination to absorb the H

atoms, therefore, improving the HER performances. Moreover, to investigate the OH-chemisorption energy of MoS<sub>2</sub>/FNS, we studied the OH adsorption on binary Fe<sub>9</sub>S<sub>8</sub> (422) and Ni<sub>9</sub>S<sub>8</sub> (422) surfaces with and without Mo doping, rather than using a disordered atomic model of FNS, due to the massive calculations it would involve (Figure S18, Supporting Information). As expected, the OH-chemisorption energy of undercoordinated Fe sites is -2.921 eV for Mo-Fe<sub>9</sub>S<sub>8</sub>, substantially lower than that of Fe<sub>9</sub>S<sub>8</sub> ( $\Delta G_{\text{OH}} = -0.940$  eV). As for Ni<sub>9</sub>S<sub>8</sub>, the OH-chemisorption energy of undercoordinated Ni sites shows the same trend as Fe<sub>9</sub>S<sub>8</sub>, which decreases from -1.839 to -2.438 eV after Mo doping. These results suggest that the OH group is prone to absorb on the undercoordinated Fe and Ni sites of Fe<sub>9</sub>S<sub>8</sub> and Ni<sub>9</sub>S<sub>8</sub>, respectively in the presence of Mo doping. Therefore, we can deduce that the MoS<sub>2</sub>/FNS coupling interfaces can boost the absorption of OH and raise the OER performances. Consequently, we propose the mechanisms of HER and OER of MoS<sub>2</sub>/FNS (Figure 5b). As mentioned above, owing to the lower chemisorption energy, the H atoms are easier to absorb on the S sites of MoS<sub>2</sub>/FNS interfaces, which decreases the Gibbs free energies of corresponding intermediates, eventually facilitating the HER performances. MoS<sub>2</sub>/FNS interfaces also exhibit the advantages of absorbing the OH groups, reducing the Gibbs free energies of corresponding intermediates (OH, OOH, and OH bonds of H<sub>2</sub>O) and therefore enhancing the OER performances.

In summary, we successfully synthesized vertical MoS<sub>2</sub> array grown on FNS/FeNi foam and other substrates with controlled arrangement by changing the reaction condition of CVD.

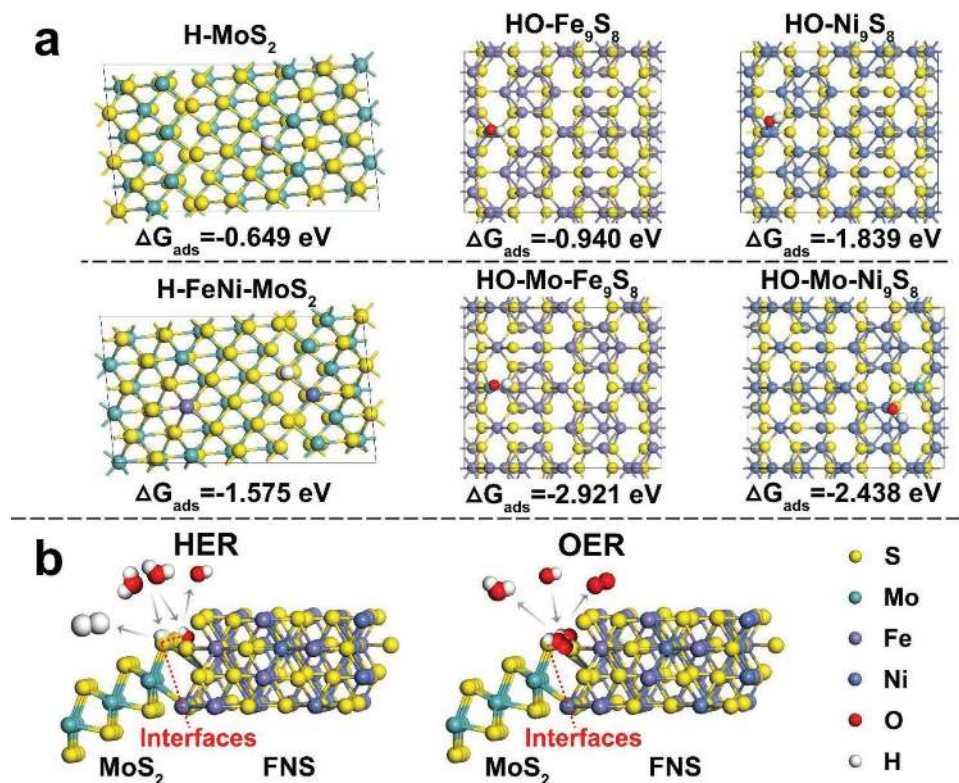


**Figure 5.** DFT models and mechanisms of MoS<sub>2</sub>, MoS<sub>2</sub>/FNS for HER and OER. a) Chemisorption models and corresponding adsorption energy of H and OH on the surfaces of MoS<sub>2</sub>, Fe<sub>9</sub>S<sub>8</sub>, Ni<sub>9</sub>S<sub>8</sub>, MoS<sub>2</sub>/FNS (Fe, Ni-MoS<sub>2</sub> model), MoS<sub>2</sub>/Fe<sub>9</sub>S<sub>8</sub> (Mo-Fe<sub>9</sub>S<sub>8</sub> model), and MoS<sub>2</sub>/Ni<sub>9</sub>S<sub>8</sub> (Mo-Ni<sub>9</sub>S<sub>8</sub> model) heterostructures. b) The mechanisms of MoS<sub>2</sub>/FNS coupling interfaces acting on HER and OER.

Further investigations demonstrated the edge-riched MoS<sub>2</sub> nanosheets have an improved effect on the different substrates for the water splitting efficiency. Among them, the MoS<sub>2</sub>/FNS/FeNi foam shows the best performance with an overpotential of 120 mV at 10 mA cm<sup>-2</sup> in HER and 204 mV at 10 mA cm<sup>-2</sup> in OER. The high-specific surface area, the ideal conductivity of FeNi foam, the coupling interfaces between MoS<sub>2</sub> and FNS, and the exposed edges of MoS<sub>2</sub> have a combined favorable effect for the electrochemical water splitting. Therefore, all these factors make the MoS<sub>2</sub>/FNS/FeNi foam be a promising material for water splitting with ordinary synthesis, inexpensive resources, and unmatched properties, and these coupling interfaces provide a valid direction for finding cheap, efficient, and clean electrodes for water splitting.

## Supporting Information

Supporting Information is available from the Wiley Online Library or from the author.

## Acknowledgements

This work was sponsored by the Thousand Talents Program for Distinguished Young Scholars from Chinese government, National Key R&D Program of China (No. 2017YFB0406000), the National Natural Science Foundation of China (51521004 and 51420105009), Start-up fund, and the Zhi-Yuan Endowed fund (T. D.) from Shanghai Jiao Tong University. H.Z. thanks the financial support from the Shanghai Sailing Program (16YF1406000) and the computing resources from Shanghai Jiao Tong University Supercomputer Center. The authors thank Instrumental Analysis Center of Shanghai Jiao Tong University for access to SEM and XPS. The authors also thank State Key Laboratory of Metal Matrix Composites for access to TEM.

## Conflict of Interest

The authors declare no conflict of interest.

## Keywords

chemical vapor deposition, coupling interfaces, hydrogen evolution, in situ grown molybdenum disulfide nanosheets, oxygen evolution

Received: May 17, 2018

Revised: June 29, 2018

Published online: August 6, 2018

- [1] S. Chen, S. S. Thind, A. Chen, *Electrochem. Commun.* **2016**, *63*, 10.
- [2] J. Zhang, T. Wang, D. Pohl, B. Rellinghaus, R. Dong, S. Liu, X. Zhuang, X. Feng, *Angew. Chem., Int. Ed.* **2016**, *55*, 6702.
- [3] P. F. Liu, S. Yang, B. Zhang, H. G. Yang, *ACS Appl. Mater. Interfaces* **2016**, *8*, 34474.
- [4] H. Jin, J. Wang, D. Su, Z. Wei, Z. Pang, Y. Wang, *J. Am. Chem. Soc.* **2015**, *137*, 2688.
- [5] W. Wang, X. Xu, W. Zhou, Z. Shao, *Adv. Sci.* **2017**, *4*, 1600371.
- [6] S. A. Grigoriev, P. Millet, V. N. Fateev, *J. Power Sources* **2008**, *177*, 281.
- [7] C. Tan, X. Cao, X. J. Wu, Q. He, J. Yang, X. Zhang, J. Chen, W. Zhao, S. Han, G. H. Nam, M. Sindoro, H. Zhang, *Chem. Rev.* **2017**, *117*, 6225.
- [8] H. Li, Y. Li, A. Aljarb, Y. Shi, L. J. Li, *Chem. Rev.* **2018**, *118*, 6134.
- [9] S. Li, S. Wang, M. M. Salamone, A. W. Robertson, S. Nayak, H. Kim, S. C. E. Tsang, M. Pasta, J. H. Warner, *ACS Catal.* **2016**, *7*, 877.
- [10] Q. Lu, Y. Yu, Q. Ma, B. Chen, H. Zhang, *Adv. Mater.* **2016**, *28*, 1917.
- [11] J. Deng, H. Li, S. Wang, D. Ding, M. Chen, C. Liu, Z. Tian, K. S. Novoselov, C. Ma, D. Deng, X. Bao, *Nat. Commun.* **2017**, *8*, 14430.
- [12] Y. Li, H. Wang, L. Xie, Y. Liang, G. Hong, H. Dai, *J. Am. Chem. Soc.* **2011**, *133*, 7296.
- [13] Y. Yang, H. Fei, G. Ruan, C. Xiang, J. M. Tour, *Adv. Mater.* **2014**, *26*, 8163.
- [14] T. F. Jaramillo, K. P. Jorgensen, J. Bonde, J. H. Nielsen, S. Horch, I. Chorkendorff, *Science* **2007**, *317*, 100.
- [15] C. Tsai, H. Li, S. Park, J. Park, H. S. Han, J. K. Nørskov, X. Zheng, F. Abild-Pedersen, *Nat. Commun.* **2017**, *8*, 15113.
- [16] Y. Yin, J. Han, Y. Zhang, X. Zhang, P. Xu, Q. Yuan, L. Samad, X. Wang, Y. Wang, Z. Zhang, P. Zhang, X. Cao, B. Song, S. Jin, *J. Am. Chem. Soc.* **2016**, *138*, 7965.
- [17] X. Zhang, Z. Lai, C. Tan, H. Zhang, *Angew. Chem., Int. Ed.* **2016**, *55*, 8816.
- [18] F. M. Pesci, M. S. Sokolikova, C. Grotta, P. C. Sherrell, F. Reale, K. Sharda, N. Ni, P. Palczynski, C. Mattevi, *ACS Catal.* **2017**, *7*, 4990.
- [19] X. Lu, Y. Lin, H. Dong, W. Dai, X. Chen, X. Qu, X. Zhang, *Sci. Rep.* **2017**, *7*, 42309.
- [20] W. Zhou, Z. Yin, Y. Du, X. Huang, Z. Zeng, Z. Fan, H. Liu, J. Wang, H. Zhang, *Small* **2013**, *9*, 140.
- [21] D. Xiong, Q. Zhang, W. Li, J. Li, X. Fu, M. F. Cerqueira, P. Alpuim, L. Liu, *Nanoscale* **2017**, *9*, 2711.
- [22] S. Deng, Y. Zhong, Y. Zeng, Y. Wang, Z. Yao, F. Yang, S. Lin, X. Wang, X. Lu, X. Xia, J. Tu, *Adv. Mater.* **2017**, *29*, 1700748.
- [23] H. Yu, Z. Yang, L. Du, J. Zhang, J. Shi, W. Chen, P. Chen, M. Liao, J. Zhao, J. Meng, G. Wang, J. Zhu, R. Yang, D. Shi, L. Gu, G. Zhang, *Small* **2017**, *13*, 1603005.
- [24] X. Yang, Q. Li, G. Hu, Z. Wang, Z. Yang, X. Liu, M. Dong, C. Pan, *Sci. China Mater.* **2016**, *59*, 182.
- [25] Y. Xie, Z. Wang, Y. Zhan, P. Zhang, R. Wu, T. Jiang, S. Wu, H. Wang, Y. Zhao, T. Nan, X. Ma, *Nanotechnology* **2017**, *28*, 084001.
- [26] P. Taheri, J. Wang, H. Xing, J. F. Destino, M. M. Arik, C. Zhao, K. Kang, B. Blizzard, L. Zhang, P. Zhao, S. Huang, S. Yang, F. V. Bright, J. Cerne, H. Zeng, *Mater. Res. Express* **2016**, *3*, 075009.
- [27] Y. Wang, Y. Zhang, Z. Liu, C. Xie, S. Feng, D. Liu, M. Shao, S. Wang, *Angew. Chem., Int. Ed.* **2017**, *56*, 5867.
- [28] B. Zhang, Y. H. Lui, L. Zhou, X. Tang, S. Hu, *J. Mater. Chem. A* **2017**, *5*, 13329.
- [29] W. Zhou, X.-J. Wu, X. Cao, X. Huang, C. Tan, J. Tian, H. Liu, J. Wang, H. Zhang, *Energy Environ. Sci.* **2013**, *6*, 2921.
- [30] M. Gao, W. Sheng, Z. Zhuang, Q. Fang, S. Gu, J. Jiang, Y. Yan, *J. Am. Chem. Soc.* **2014**, *136*, 7077.
- [31] M. A. Oliver-Tolentino, J. Vázquez-Samperio, A. Manzo-Robledo, R. d. G. González-Huerta, J. L. Flores-Moreno, D. Ramírez-Rosales, A. Guzmán-Vargas, *J. Phys. Chem. C* **2014**, *118*, 22432.
- [32] Z. Xing, X. Yang, A. M. Asiri, X. Sun, *ACS Appl. Mater. Interfaces* **2016**, *8*, 14521.
- [33] Y. H. Chang, C. T. Lin, T. Y. Chen, C. L. Hsu, Y. H. Lee, W. Zhang, K. H. Wei, L. J. Li, *Adv. Mater.* **2013**, *25*, 756.
- [34] T. Yamashita, P. Hayes, *Appl. Surf. Sci.* **2008**, *254*, 2441.
- [35] D. Voiry, R. Fullon, J. Yang, E. S. C. de Carvalho Castro, R. Kappera, I. Bozkurt, D. Kaplan, M. J. Lages, P. E. Batson, G. Gupta, A. D. Mohite, L. Dong, D. Er, V. B. Shenoy, T. Asefa, M. Chhowalla, *Nat. Mater.* **2016**, *15*, 1003.

- [36] T. Shinagawa, A. T. Garcia-Esparza, K. Takanabe, *Sci. Rep.* **2015**, *5*, 13801.
- [37] P. A. DeSario, C. N. Chervin, E. S. Nelson, M. B. Sassin, D. R. Rolison, *ACS Appl. Mater. Interfaces* **2017**, *9*, 2387.
- [38] U. Y. Qazi, C. Z. Yuan, N. Ullah, Y. F. Jjiang, M. Imran, A. Zeb, S. J. Zhao, R. Javaid, A. W. Xu, *ACS Appl. Mater. Interfaces* **2017**, *9*, 28627.
- [39] F. Hu, S. Zhu, S. Chen, Y. Li, L. Ma, T. Wu, Y. Zhang, C. Wang, C. Liu, X. Yang, L. Song, X. Yang, Y. Xiong, *Adv. Mater.* **2017**, *29*, 1606570.
- [40] W. Ma, R. Ma, C. Wang, J. Liang, X. Liu, K. Zhou, T. Sasaki, *ACS Nano* **2015**, *9*, 1977.
- [41] X. Long, J. Li, S. Xiao, K. Yan, Z. Wang, H. Chen, S. Yang, *Angew. Chem., Int. Ed.* **2014**, *53*, 7584.
- [42] J. Luo, J. H. Im, M. T. Mayer, M. Schreier, M. K. Nazeeruddin, N. G. Park, S. D. Tilley, H. J. Fan, M. Gratzel, *Science* **2014**, *345*, 1593.